The exocytotic fusion pore modeled as a lipidic pore

C. Nanavati, V. S. Markin,* A. F. Oberhauser, and J. M. Fernandez
Department of Physiology and Biophysics, Mayo Foundation, Rochester, Minnesota 55905 USA; and
*The Frumkin Institute of Electrochemistry, Academy of Sciences of Russia, Moscow, Russia

ABSTRACT Freeze-fracture electron micrographs from degranulating cells show that the lumen of the secretory granule is connected to the extracellular compartment via large (20 to 150 nm diameter) aqueous pores. These exocytotic fusion pores appear to be made up of a highly curved bilayer that spans the plasma and granule membranes. Conductance measurements, using the patch-clamp technique, have been used to study the fusion pore from the instant it conducts ions. These measurements reveal the presence of early fusion pores that are much smaller than those observed in electron micrographs. Early fusion pores open abruptly, fluctuate, and then either expand irreversibly or close. The molecular structure of these early fusion pores is unknown. In the simplest extremes, these early fusion pores could be either ion channel like protein pores or lipidic pores. Here, we explored the latter possibility, namely that of the early exocytotic fusion pore modeled as a lipid-lined pore whose free energy was composed of curvature elastic energy and work done by tension. Like early exocytotic fusion pores, we found that these lipidic pores could open abruptly, fluctuate, and expand irreversibly. Closure of these lipidic pores could be caused by slight changes in lipid composition. Conductance distributions for stable lipidic pores matched those of exocytotic fusion pores. These findings demonstrate that lipidic pores can exhibit the properties of exocytotic fusion pores, thus providing an alternate framework with which to understand and interpret exocytotic fusion pore data.

INTRODUCTION

Exocytosis is a highly regulated process in which the well-separated membranes from the plasma and secretory granule are brought together in a highly localized region and fused (Chandler and Heuser, 1980; Ornberg and Reese, 1981). During a fusion event, exocytotic fusion pores, which form an aqueous connection between the granule lumen and the extracellular space, expand rapidly. Exposure of the granule core to the extracellular saline causes the decondensation of the granule core, resulting in the secretion of granule contents to the extracellular space.

The molecular structure of the exocytotic fusion pore is unknown, though its properties have been studied from the instant it forms a conducting channel until it ceases to exist as a distinguishable entity. Electrical measurements of fusion pore conductance using the patch-clamp technique reveal that fusion pores open abruptly with an initial conductance of a few hundred picosiemens (Spruce et al., 1990). Their conductance fluctuates around some value before either returning to zero, indicating pore closure, or increasing to an immeasurably large value (>10 nS), indicating irreversible expansion of the fusion pore (Breckenridge and Almers, 1987; Alvarez de Toledo and Fernandez, 1988; Spruce et al., 1990). These electrically detectable fusion pores have a calculated diameter < 2.5 nm and are therefore referred to as early fusion pores (Spruce et al., 1990). Freeze-fracture electron micrographs of degranulating mast cells show water-filled pores (diameter 20–150 nm) connecting the granule lumen and the extracellular compartment. These larger, late fusion pores, which must succeed the fusion pores detected by the patch-clamp technique, are surrounded by a highly curved membrane that spans the cellular and granular bilayers. Rapid expansion of these late fusion pores results in the release of secretory vesicle contents (Chandler and Heuser, 1980; Ornberg and Reese, 1981). As shown by the freeze-fracture experiments, late fusion pores are made up of lipids in a bilayer configuration.

Due to their small size, early fusion pores are not observed with the freeze-fracture technique. As a result, their molecular structure is unknown. Here we ask whether the early exocytotic fusion pore could be a lipidic pore. In other words, do lipidic pores possess the properties of the early fusion pore? To answer this question, we derive an expression for the free energy of a lipidic pore that is determined by the properties of the lipids themselves and the forces that are present within the bilayer during the lifetime of the pore. The most important intrinsic property of a lipid is its shape, which determines whether a given lipid will spontaneously form a bilayer (e.g., phosphatidylcholine), micelle (e.g., single-stranded lecithin), or inverted cylinder (e.g., unsaturated phosphatidylethanolamine). Helfrich (1973) quantified the concept of lipid shape in terms of spontaneous curvature and proposed that a quadratic, Hookean curvature energy was associated with deviations of the membrane curvature from the spontaneous curvature. He and others showed that curvature energy is an important determinant of the spontaneous shapes of both red blood cells and artificial bilayers (Deuling and Helfrich, 1976, 1977; Markin, 1981; Kas and Sack-

Dr. Nanavati's present address is Department of Cell Biology, Duke University Medical Center, Durham, NC 27710.

V. S. Markin is a visiting scientist. His current address is Department of Cell Biology, University of Texas, Southwestern Medical Center, 5323 Harry Hines Blvd., Dallas, TX 75235.

Abbreviations used: PC, phosphatidylcholine; PE, phosphatidylethanolamine; DMPE, dimyristoyl-phosphatidylethanolamine; DMPC, dimyristoyl-phosphatidylcholine; DLPE, dilauroyl-phosphatidylethanolamine; DOPE, dioleoyl-phosphatidylethanolamine; DOPC, dioleoyl-phosphatidylcholine.

0006-3495/92/10/1118/15 $2.00

mann, 1991). In addition to lipid shape, membrane tension, the mechanism by which all known experimental interventions induce fusion in artificial bilayer systems, also affects the fate of the fusion pore (Helm et al., 1992). Monck et al. (1990) provided evidence that the granule membrane of mast cells is under tension. Since this tension lasts through the lifetime of the fusion pore, we included its contribution to the free energy.

We found that a lipidic pore whose free energy was composed of elastic bending energy and tension, could, like an early exocytotic fusion pore, open abruptly, fluctuate, and then expand irreversibly. Closure of fluctuating fusion pores that accounts for 20–30% of all fusion events could be explained as a result of slight changes in lipid composition and therefore spontaneous curvature. Using experimentally or literature-derived values for the various physical parameters, we could fit the conductance distributions for fluctuating exocytotic fusion pores with those predicted for lipidic pores. We have therefore demonstrated that lipidic pores can behave like early fusion pores. A preliminary report of this work appeared in abstract form (Nanavati et al., 1992).

THEORETICAL MODEL

Lipidic pores are formed during the fusion of two phospholipid bilayers, which occurs under appropriate fusogenic conditions. Fusogenic manipulations increase lateral bilayer tension and part lipid head groups, exposing hydrocarbon tails, thus bypassing repulsive forces and increasing attractive hydrophobic forces between the exposed tails of the phospholipids in the apposed monolayers of the two bilayers (Helm et al., 1992). This results in the formation of a single, hemifused bilayer that connects the two membranes without connecting the aqueous compartments on either side. A pore through this hemifused bilayer forms the first aqueous connection across the membranes being fused. The expansion of this pore results in complete fusion. The question addressed in this paper is whether such a lipidic pore could display the same electrical characteristics as the early fusion pore. To understand how lipidic pores behave, we need (*a*) a description of the geometry for a pore, (*b*) the conductance of a pore since conductance is the measurable property of an early fusion pore, and (*c*) an expression for the energy of a lipid pore since energy governs behavior. Following Markin et al. (1984), we modeled a lipidic pore as shown in Fig. 1 *A*. The pore was generated by revolving a semicircle of radius, b, about an external diameter (distance a). In principle, such a lipid pore could span either the two bilayers of the membranes being fused or the single hemifused bilayer formed as a fusion intermediate (Fig. 1, *B* and *C*, respectively). The surface of revolution shown in Fig. 1 *A* corresponds to the neutral surface generated by revolving the dashed lines in Fig. 1, *B* and *C*, and does not correspond to the surface of the pore in contact with aqueous solutes. Depending on the type of pore, the geometrical parameters, a and b, are related to pore radius (r), bilayer thickness ($2h$), and interbilayer distance (d) by $a = r + h/2$; $b = h/2$, for a pore spanning one bilayer; and $a = r + h$; $b = h + d/2$, for a pore spanning two bilayers. The theoretical development is the same for the two types of pores, both of which have been described in the literature (Markin et al., 1984; Siegel, 1986; Song et al., 1991; Helm et al., 1992). Freeze-fracture data suggest that late exocytotic fusion pores are lipidic pores that span two bilayers, while artificial bilayer fusion experiments suggest that early fusion pores are lipidic pores through a single bilayer. The main conclusions of this paper are valid regardless of pore geometry, although numerical values depend on geometry.

Pore conductance

The total resistance of a lipid pore of radius, r, and length, L, with the geometry of Fig. 1 *A* is (derived in the Appendix)

$$R_{\text{total}} = \frac{\rho}{\pi}\frac{L}{r(r+L)}\left\{1 + \frac{L}{\sqrt{r(r+L)}}\arctan\sqrt{\frac{r+L}{r}}\right\} + \frac{\rho}{2r+L}. \quad (1)$$

Pore conductance G_p is the inverse of R_{total}.

Pore energy

The behavior of a lipidic pore is determined by its energy. Changes that result in lower pore energy occur with a higher probability than those that result in a higher final energy. The elastic bending energy and work done by tension are included in this analysis. The bending energy, W_b, accounts for the spontaneous curvature, J_s, of lipids lining the pore. It is proportional to the square of the difference between the mean curvature of a lipidic pore and the spontaneous curvature, J_s, of the lipids lining the pore. For a lipidic pore with the geometry of Fig. 1 *A* and a bending modulus, k_c, W_b is given by Markin et al. (1984) (also see Appendix)

$$W_b = 2\pi k_c\left\{\pi J_s a + \frac{2(b+a)^2}{b\sqrt{a(a+2b)}}\arctan\sqrt{\frac{a+2b}{a}} + \left(\frac{\pi}{2} - 4\right)bJ_s - 4\right\}. \quad (2)$$

For arbitrary pore radius, the relationship between energy and radius is a complicated function that depends on spontaneous curvature. As shown by the solid curves of Fig. 2, the bending energy (*a*) increases with radius (Fig. 2 *A*, curve *1*), (*b*) decreases with radius (Fig. 2 *C*, curve *1*), or (*c*) displays a minimum at some radius (Fig. 2 *B*, curve *1*). The type of energy dependence is determined by spontaneous curvature and predicts the most probable behavior of a lipidic pore: a structure whose energy increases with radius is unlikely to form (Fig. 2

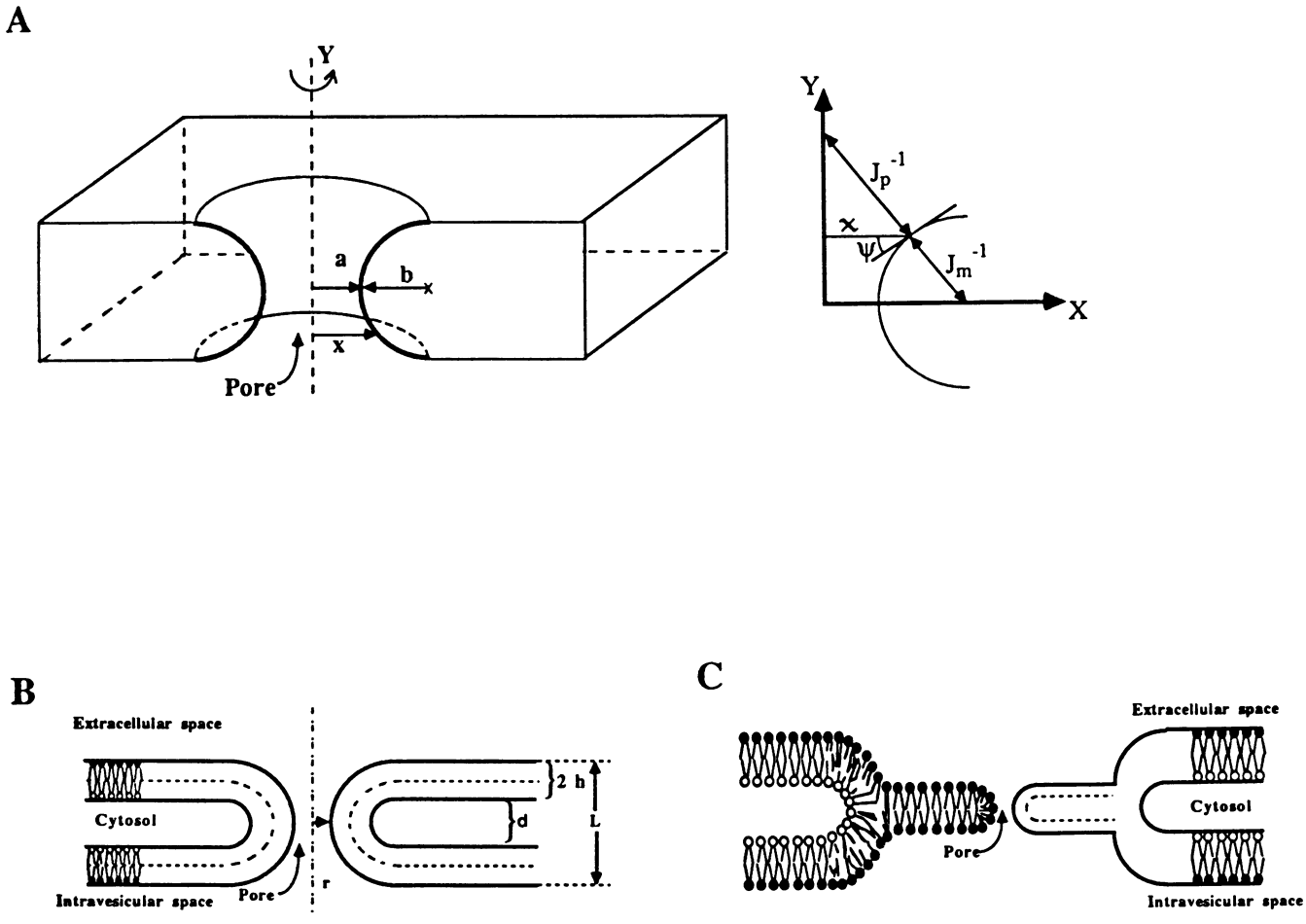

FIGURE 1 (*A*) Geometry of a pore that is generated by revolving the semicircles (*thick curves*) about the axis of revolution, *Y*. a = radius of the narrowest part of the pore; b = radius of the generating semicircles; x = shortest distance between the axis of revolution and a point on the semicircle. Inset shows the same geometry with the angle and radii of curvatures. J_p^{-1} and J_m^{-1} are the parallel and meridional radii of curvature, respectively. $\psi(x)$ is the angle between the tangent to the semicircle at the point (x, y) and the horizontal axis. (*B*) A pore spanning two bilayers and the space between them. h = monolayer thickness, d = interbilayer distance, L = pore length = $4h + d$. (*C*) A pore spanning the single bilayer formed on hemifusion of the fusing bilayers ($L = 2h$).

A), one whose energy decreases with radius is likely to expand continuously after opening (Fig. 2 *C*), and one whose energy has a minimum is likely to open with a radius that fluctuates around an equilibrium radius (Fig. 2 *B*). Calculating the first derivative of W_b with respect to radius, we find that the curvature energy of a lipidic pore through a 4-nm-thick bilayer increases monotonically when $J_s \geq -0.3$ nm^{-1}, displays a minimum when J_s lies between -0.3 and -0.5 nm^{-1}, or decreases monotonically when $J_s \leq -0.5$ nm^{-1}. As J_s decreases from -0.3 to -0.5 nm^{-1}, the equilibrium radius increases from 0 to 14.7 nm. To put these numbers into perspective, a spontaneous curvature of -0.5 nm^{-1} means that lipids spontaneously form inverted hexagonal cylinders with an average radius of 2 nm. Phospholipids, their analogs, and biological membrane extracts spontaneously form inverted cylinders with radii between 0.5 and 5 nm (Luzzati and Husson, 1962; Tate and Gruner, 1987; Rand et al., 1990; Leventis et al., 1991).

To account for the flow of lipids that begins when the exocytotic fusion pore opens and stops when the pore closes, we included $W_{tension}$, the contribution of tension, γ, to the free energy. $W_{tension}$ is given by

$$W_{tension} = -2\pi\gamma(a^2 - (\pi - 3)b^2 - (\pi - 2)ab).$$

The total free energy is the sum of W_b and $W_{tension}$. Since lateral tension forms pores in bilayers, $W_{tension}$ decreases as pore radius increases and therefore competes with W_b, which sometimes stabilizes pores of zero or finite radii (Fig. 2, *A* and *B*, curve *1*). With a large enough tension, all pores expand irreversibly without fluctuating (Fig. 2 *B*, curve *3*). Such irreversible expansion without stable fluctuations occurs when the work done by tension dominates the free energy at all radii. For smaller values of tension, the total energy has a minimum followed by a maximum (Fig. 2, *A* and *B*, curve *2*). The maximum represents an energy barrier whose height depends on

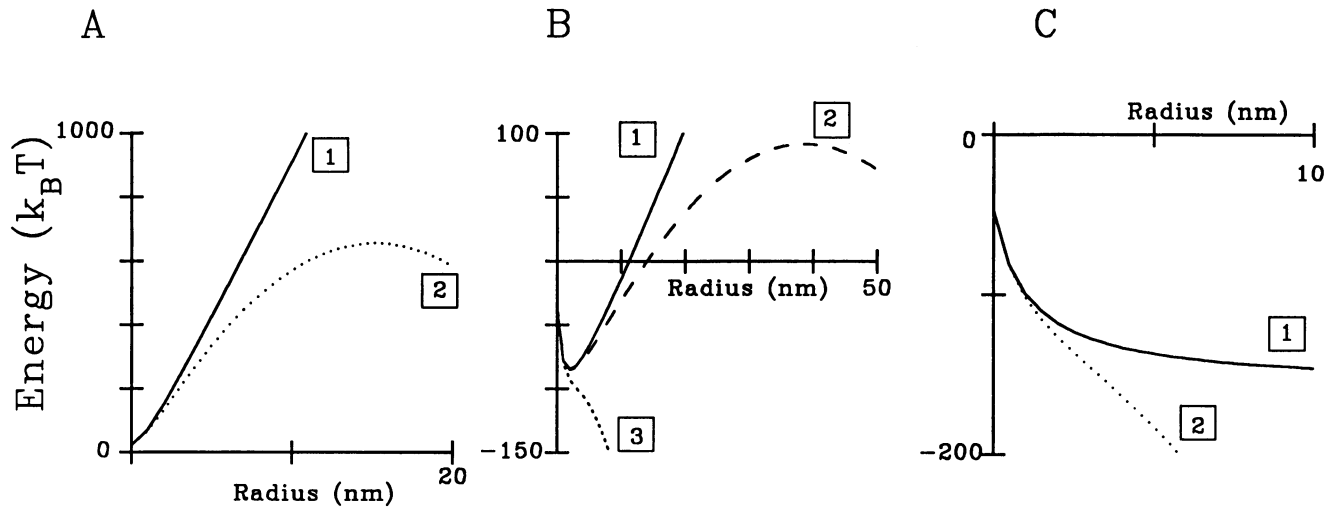

FIGURE 2 Energy of a lipidic pore spanning a single bilayer in the absence (*solid*) or presence (*dashed* or *dotted curves*) of tension. The spontaneous curvatures and tensions used to generate these curves were (*A*) -0.3 nm^{-1} with no tension (curve *1*) or a tension of 2 mN/m (curve *2*); (*B*) -0.475 nm^{-1} with no tension (curve *1*), a tension of 0.1 mN/m (curve *2*), or a tension of 1 mN/m (curve *3*); (*C*) -0.5 nm^{-1} (curve *1*) with a tension of 1 mN/m (curve *2*).

spontaneous curvature, tension, and elastic bending modulus. Once this barrier is overcome, irreversibly expanding pores become energetically favorable.

As tension increases, the height of the energy barrier decreases until, finally, free energy is a decreasing function of radius (Fig. 2 *B*, curve *3*). For a given tension, as the spontaneous curvature decreases from -0.3 to -0.5 nm^{-1}, the distance between the equilibrium and barrier radii decreases and the barrier height (difference between the energy maximum and minimum) decreases. The latter quantity determines the probability of irreversible expansion and suggests that for a given bilayer tension, large stable pores are more likely to expand irreversibly than small stable pores. However, when pore area (or diameter) increases, bilayer tension decreases. Thus, small pores with a larger bilayer tension and a smaller barrier height could expand irreversibly with a probability comparable with that of larger pores that have a smaller bilayer tension. We could neither confirm nor deny this prediction since the number of analyzable fusion events was limited (see Methods for criteria).

Although tension does not significantly affect the equilibrium radius, it does increase the width of the energy well (compare Fig. 2 *B*, curves *1* and *2*). The distribution of pore radii and therefore of pore conductance is determined by pore energy with the equilibrium radius corresponding to the most probable radius and the width of the energy well corresponding to the width of the distribution. Based on its effects on pore energy, tension will alter the width of the pore conductance distributions without affecting the location of the most probable conductance level. For a given bending modulus, tension determines the mean conductance of the largest stable fusion pore. For instance, for the bending modulus used for the calculations in this paper, the largest mean conductance for a stable conducting pore decreases from 31 to 6.7 nS when the tension increases from 0 to 0.1 mN/m.

Fig. 3 is a phase diagram that summarizes the dependence of energy on pore radius and spontaneous curvature for a pore through a 4-nm-thick bilayer subject to a tension of 0.1 mN/m. There are three regions on the

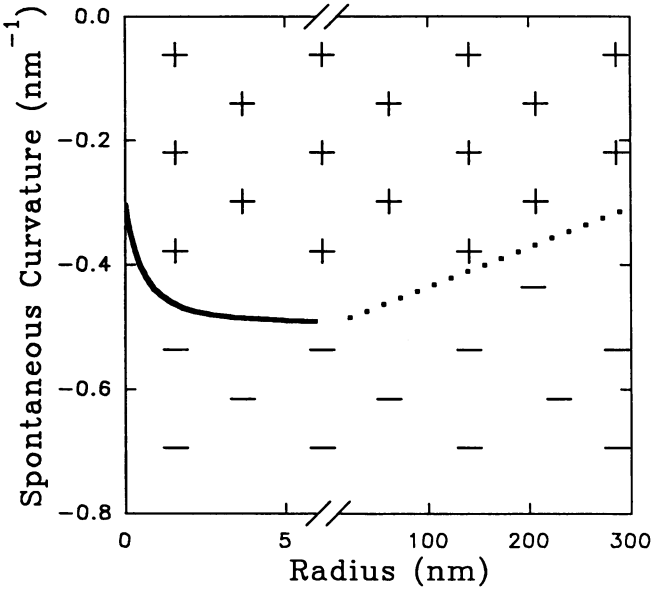

FIGURE 3 Phase diagram that summarizes the dependence of energy on pore radius and spontaneous curvatures. +, spontaneous curvatures and radii for which the energy increases with increasing radius; −, spontaneous curvatures and radii for which the energy decreases with increasing radius; *curves*, pore radius at which for a given spontaneous curvature the energy has a minimum (*solid curve*) or maximum (*dotted curve*).

phase-diagram that, for a fixed spontaneous curvature, correspond to (*a*) energy increasing with increasing radius (plus), (*b*) energy decreasing with increasing radius (minus), and (*c*) energy remaining constant for small changes in pore radius (*solid* and *dotted curves*). The solid and dashed curves show spontaneous curvature versus the radius corresponding to an energy minimum or maximum, respectively. By drawing a horizontal line at the appropriate J_s, we can predict the dependence of energy on pore radius. For $J_s = -0.6\ nm^{-1}$, this horizontal line remains in the region denoted by minus signs, indicating that energy is a decreasing function of radius so the pore will expand irreversibly. For $J_s = -0.475\ nm^{-1}$, this horizontal line crosses three regions. For small radii, this line is in the region denoted by minus signs, indicating that energy decreases with increasing radius. At a radius of 2 nm, this line crosses the solid curve and enters the region denoted by plus signs, implying that energy now increases with increasing radius. Finally, at a radius of 40 nm, this line crosses the dashed curve and enters the region denoted by minus signs, indicating that energy once again decreases with radius. So, for $J_s = -0.475\ nm^{-1}$, free energy decreases with increasing radius for radii <2 nm, increases with increasing radius for radii between 2 and 40 nm, and once again decreases with increasing radius for radii > 40 nm. The free energy therefore has a minimum and a maximum at 2 and 40 nm, respectively. Although this figure does not provide information on the depth of the energy well or the height of the energy barrier, it does tell us whether such wells or barriers exist and what radii they correspond to.

METHODS

Cell isolation and solutions

Peritoneal mast cells were harvested from beige mice (bg^j/bg^j; Jackson Laboratories, Bar Harbor, ME) as described (Alvarez de Toledo and Fernandez, 1990). Cells were kept in a solution containing (mM) 136 NaCl, 2.5 KOH, 1.4 NaOH, 0.9 $MgCl_2$, 1.8 $CaCl_2$, 45 $NaHCO_3$, 6 glucose, 0.4 phosphate, and 9 *N*-2-hydroxyethylpiperazine-*N'*-2-ethane sulfonic acid (Hepes) (pH 7.25, 310 mmol/kg). For patch-clamp experiments, the extracellular medium contained (mM) 150 NaCl, 2.8 KOH, 1.5 NaOH, 1 $MgCl_2$, 2 $CaCl_2$, 25 glucose, and 10 Hepes (pH 7.25, 310 mmol/kg), whereas the pipette solution contained (mM) 140 K-glutamate, 7 $MgCl_2$, 3 KOH, 0.2 adenosine triphosphate, 1 $CaCl_2$, 10 ethyleneglycol-bis(β-aminoethyl ether)-*N,N'*-tetraacetic acid, 0.01 GTPγS, and 10 Hepes (pH 7.25, 300 mmol/kg).

Cell capacitance measurements

The cell membrane capacitance was measured using the whole cell mode of the patch-clamp technique (Hamill et al., 1981) in conjunction with a digital phase detector (Joshi and Fernandez, 1988) implemented on a system consisting of a Compaq 386/25 microcomputer and a data acquisition interface (Indec, Sunnyvale, CA). The phase was periodically adjusted using the phase tracking technique (Fidler and Fernandez, 1989). After applying a sinusoidal voltage (833 Hz, 54 mV peak to peak) to the stimulus input of the patch-clamp amplifier (EPC-7; List Electronics, Darmstadt, Germany), the current was measured at two different phase angles, ϕ and $\phi - \pi/2$, relative to the stimulus. The phase detector was aligned so that the output at $\phi - \pi/2$ reflected changes in the real part of the cell admittance ($Re(\Delta Y)$), whereas the output at ϕ reflected changes in the imaginary part of the admittance, ($Im(\Delta Y)$). The cell surface area was calculated from the membrane capacitance assuming a membrane capacity of 10 $fF/\mu m^2$. A 100-fF calibration signal for the capacitance trace was obtained by switching a 100 Ω resistor into the C-slow compensation circuitry of the patch-clamp amplifier. Since a 10-kΩ excursion on the slow capacitance circuitry corresponds to 10 pF, the 100 Ω resistor was equivalent to a 1% change (i.e., 100 fF) in the capacitance. The membrane capacitance was calculated once every 15 ms.

Calculation of pore conductance and granule capacitance

Fig. 4 *A* shows the equivalent circuit for a patch-clamped mast cell with a fusing granule. The granule lumen and extracellular compartment are connected via an ion-conducting pore with an equivalent conductance, G_p. This fusion pore is in series with the granule membrane capacitance, C_g. The cell membrane (capacitance, C_m) and granule provide alternate paths to ground, thus behaving like electrical elements in parallel. On fusion of a granule, the real and imaginary parts of the cell membrane admittance change as shown in Fig. 4 *A*. For irreversible fusion events, the granule capacitance, C_g, was measured directly from the change in the current measured at ϕ, i.e., from the change in $Im(\Delta Y)$ while for reversible events, it was computed as

$$C_g = 2\pi f \text{Average}\,[(\text{Re}(\Delta Y_i)^2 + \text{Im}(\Delta Y_i)^2)/\text{Im}(\Delta Y_i)]. \quad (3a)$$

For both reversible and irreversible events, $G_{p,i}$, the pore conductance, was computed point-by-point as

$$G_{p,i} = 2\pi f C_g(\text{Im}(\Delta Y_i)/\text{Re}(\Delta Y_i)), \quad (3b)$$

where f, the frequency of the sine wave, was 833 Hz.

For irreversible events, we found that estimates of G_p using $Im(\Delta Y)$ alone (Spruce et al., 1990) were very sensitive to noise (both in the baseline and once fusion was complete). On the other hand, estimates of G_p calculated as in Eq. 3b were very sensitive to $Re(\Delta Y)$, particularly when $Re(\Delta Y)$ was small. We therefore calculated $G_{p,i}$ as long as both $Re(\Delta Y)$ and $Im(\Delta Y)$ were greater than three standard deviations of the baseline. Typically, one standard deviation of the baseline was 2 fF ($Im(\Delta Y)$) and 10 pS ($Re(\Delta Y)$).

For this analysis, we selected events for which $Re(\Delta Y)$ at the end of the event was within three standard deviations of its value before the event. At the end of transient events, due to membrane uptake (Monck et al., 1990), $Im(\Delta Y)$ was often less than its value before the event. To compute G_p, we always chose the baseline for $Im(\Delta Y)$ at the pre-event level. In some events, the baseline of $Re(\Delta Y)$ and/or $Im(\Delta Y)$ drifted steadily. This steady drift was subtracted before calculating G_p. Since the optimal phase angle was changing during a fusion event, the size of a granule was slightly underestimated at the end of an irreversible event. Consider the case when the optimal phase angle was chosen at the beginning of an experiment on a 3 pF cell (access conductance of 100 nS, membrane conductance of 1 nS) and was left unchanged through several fusion events. If a granule fuses when the capacitance has increased to 5 pF, the error in the size of the capacitance would be 3% (Joshi and Fernandez, 1988). Since the pore conductance is proportional to the granule capacitance, the pore conductance will be underestimated by this amount.

Fits of histograms

The theory developed to predict pore conductance distributions assumes pore energy is near the equilibrium value. To relate the theory with the experimental data, we chose events for which the lifetimes in a quasi-steady-state level were longer than 300 ms (20 points). The con-

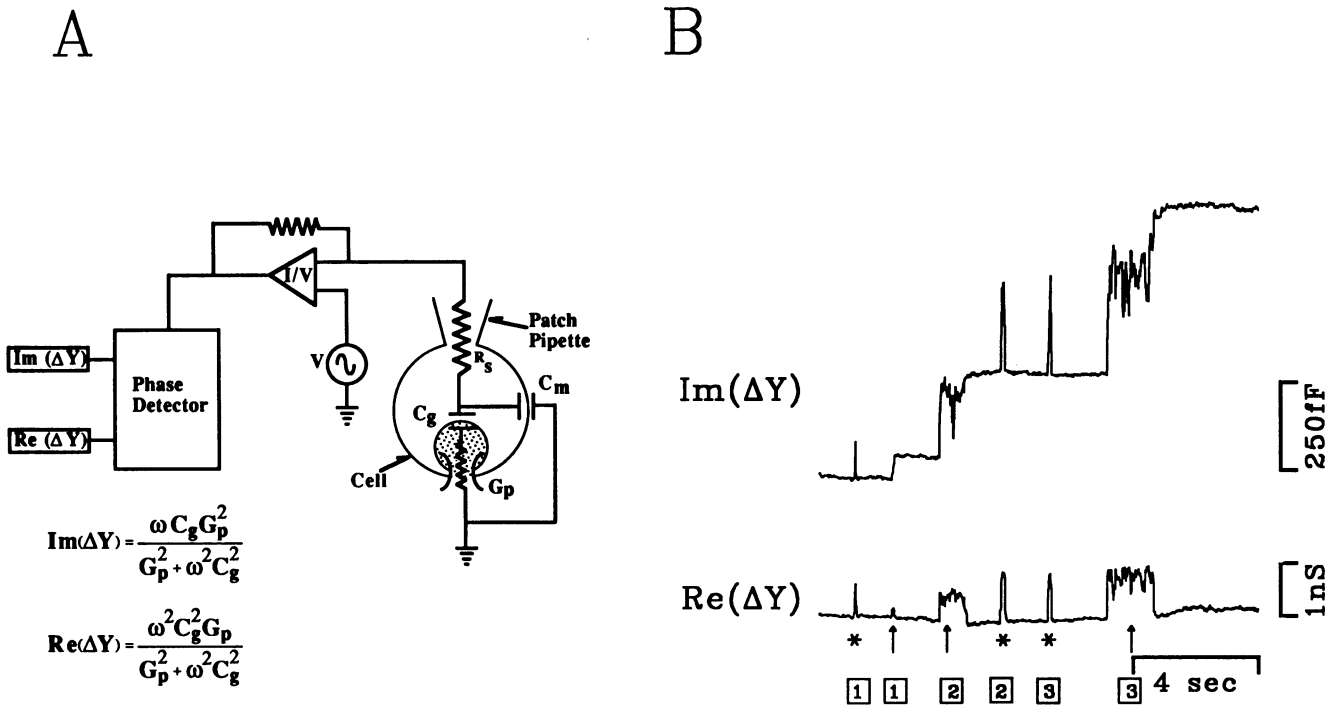

FIGURE 4 (*A*) Equivalent circuit for a patch-clamped cell with an exocytosing granule. C_m, C_g = cell membrane and granule membrane capacitance; R_s = pipette series resistance; G_p = pore conductance; V = applied sinusoidal voltage; I/V = current to voltage converter. (*B*) Experimentally obtained data shows the two outputs of the phase-detector. Both transient (*asterisks*) and irreversible (*arrows*) fusion events were observed in this 15-s trace from a degranulating beige mouse mast cell. The event denoted by asterisk 1 probably corresponds to the transient fusion of the granule that fused as arrow 2; the events denoted by asterisks 2 and 3 probably correspond to transient fusions of the granule that fused as arrow 3.

ductance was quasi-steady if the mean remained constant except for random fluctuations. We performed fits of experimentally obtained histograms by varying the spontaneous curvature keeping all other parameters fixed. Out of 25 transient events and 48 irreversible events for which we could compute a fusion pore conductance, 11 transient events and 9 irreversible events fit the above criteria for duration of a measurable, quasi-steady-state fusion pore conductance. Of these events, there were two transient events and one irreversible event in which the fusion pore conductance exhibited two or more stable conductance state. By analyzing each conductance state separately from 20 analyzable events, we constructed 24 histograms and calculated 24 points for the mean-variance plot on Fig. 8.

EXPERIMENTAL RESULTS

Measurements

Fig. 4 *B* shows the changes in the imaginary and real parts of the cell admittance during the degranulation of a beige mouse mast cell. Fusion, either transient or irreversible, was always accompanied by a change in $Im(\Delta Y)$. In this particular example, each change in $Im(\Delta Y)$ was also accompanied by a transient change in $Re(\Delta Y)$, which increased abruptly at the beginning of an event and returned to its prefusion level after an event. The end of an event signaled either irreversible fusion or closure of the fusion pore. These two types of events could be distinguished by examining changes in the imaginary part of the admittance which increased either irreversibly (*arrows*) or transiently (*asterisks*). The duration of different fusion events shown here ranged from a few milliseconds to seconds. The first brief irreversible event resulted from the rapid fusion of a 75 fF granule (arrow *1*). The noise in the imaginary trace remained unchanged before, during, and after this event. The remaining two irreversible events lasted 0.8 and 1.6 s, respectively (arrows *2* and *3*). Although the noise in the imaginary trace remained unchanged before and after these events, it increased during these events. The source of this increased noise was a fusion pore with a finite, non-zero conductance. Since the three transient events in this trace were short (<5 points per event), the capacitance, calculated using Eq. 3a, could not be determined (averaged) accurately.

Analysis

Fig. 5, *A* and *B*, shows examples of irreversible and transient fusion events and the type of analysis performed on each. The conductance of the fusion pore, G_{pore}, for each event was computed point by point using Eq. 3b and is shown in the bottom traces of Fig. 5, *A* and *B*. For the irreversible event of Fig. 5 *A*, the conductance of the fusion pore was initially small (500 pS) and remained small for ~300 ms, before increasing slightly. After a total of 500 ms, the fusion pore suddenly expanded irreversibly, resulting in an immeasurably large pore conductance. On irreversible expansion of the fusion pore, the projection on $Re(\Delta Y)$ abruptly dropped to zero. The

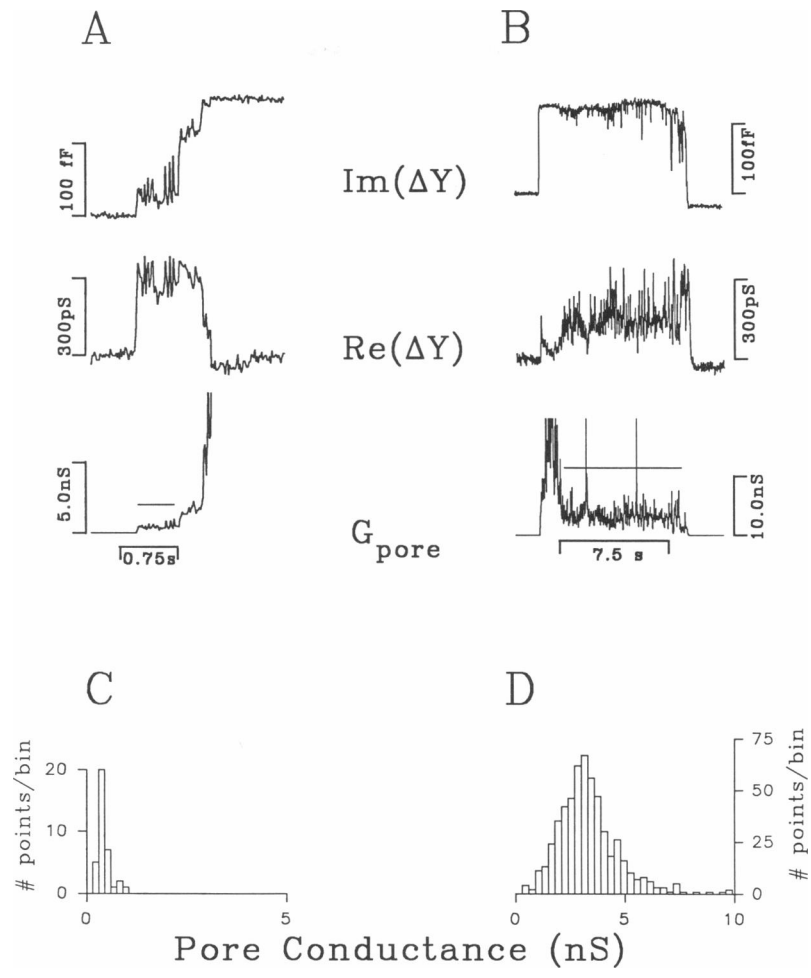

FIGURE 5 Conductance of the fusion pore (third trace) of an irreversible fusion event (*A*) and a transient event (*B*) calculated from the raw data (top trace and middle trace). The actual values for the pore conductance in *B* are unreliable once the conductance exceeds ~12 nS. The resolution for *B* was calculated as follows: the capacitance of the fusing granule was 125 fF. The noise on the imaginary and real traces was 1.4 fF and 10.3 pS. Using the expression for Re(ΔY) from Fig. 4 *A*, a pore conductance of 12.5 nS corresponds to Re(ΔY) = 31 pS (within 3 standard deviations of the noise in Re(ΔY)). (*C* and *D*) Histograms of fusion pore conductance for the regions marked by a line in *A* and *B*, respectively. Bin width was 150 pS for both histograms. The ordinate is the time (= # points × 15 ms/point) that the conductance was between G_p and G_p + 150 pS.

transient fusion event shown in Fig. 5 *B* was unusually long (10.8 s). The first indication of pore formation in this case was a transient increase in Re(ΔY) accompanied by an abrupt increase in Im(ΔY). The corresponding conductance was >12 nS, suggesting the presence of either one large fusion pore or several smaller fusion pores. For the next second, the conductance of the fusion pore remained large and then suddenly started fluctuating as shown by the increased noise in both Im(ΔY) and Re(ΔY). It then fluctuated around 5 nS for 8 s, decreased to ~500 pS, and then closed abruptly. On closure, the projection on Im(ΔY) returned to a level that was clearly below (by 18 fF) the prefusion basal level. This reduction in the capacitance of the plasma membrane was described by Monck et al. (1990). Re(ΔY) returned to a slightly lower level at the end of both the irreversible and the transient fusion events shown here. This was neither a significant nor a reproducible shift. After a fusion event (transient or irreversible), Re(ΔY) sometimes returned to its prefusion levels and sometimes to levels that were slightly larger or smaller than prefusion levels. These changes probably reflect changes in pipette series resistance. Re(ΔY) is very sensitive to such changes, whereas Im(ΔY) is insensitive to such changes (Joshi and Fernandez, 1988).

Fig. 5, *C* and *D*, are pore conductance histograms for the events shown in Fig. 5, *A* and *B*, respectively. The histograms were constructed for the periods marked by solid lines above the pore conductance. The ordinate of the histograms shows the amount of time (= number of points × 15 ms/point) when the conductance was between G_p and $G_p + dG_p$. The distribution of Fig. 5 *C* was narrow with a peak around 500 pS, whereas the distribution of Fig. 5 *D* was considerably broader with a peak around 5 nS. At first glance it might appear that smaller fluctuating pores (small mean conductance) with smaller fluctuations are more likely to expand irreversibly than larger fluctuating pores. However, the data do

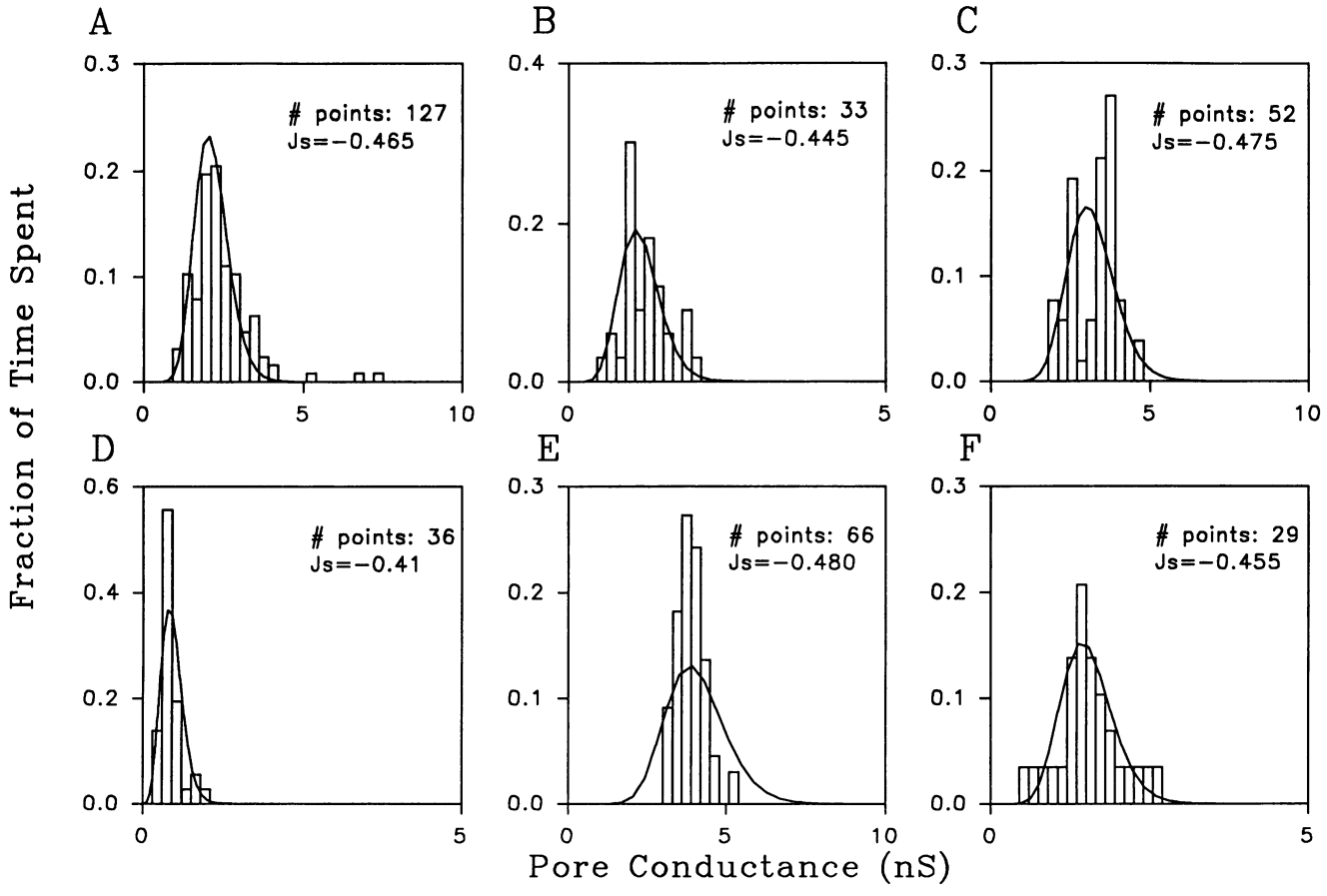

FIGURE 6 Comparison of theoretical predictions with experimental data for irreversible fusion events. Fusion pore conductance histograms (*bars*) for six irreversible events were fit to theoretically predicted distributions (*continuous curves*) assuming a pore in a bilayer ($k_c = 1 \times 10^{-12}$ ergs, $h = 2$ nm). Tension was 0.1 mN/m and the bin width was 150 pS (*A, C,* and *E*) or 300 pS (*B, D,* and *F*). The spontaneous curvature for the fits and the number of points in each histograms are specified. The distributions shown in Figs. 6 *B* and 7 *C* are from an irreversible and a transient fusion event in the same cell.

not support this conclusion. Figs. 6 and 7 show fusion pore conductance histograms for several irreversible and transient events. At the end of a fusion event, fusion pores expanded irreversibly or closed independent of mean pore conductance (e.g., irreversible, Fig. 6, *C* and *D;* transient, Fig. 7, *E* and *F*). The conductance at any time during a fusion event was insufficient to predict the fate of a given fusion pore. For instance, the fusion pore of Fig. 5 *A* expanded irreversibly once its conductance exceeded ~2 nS, whereas the fusion pore of Fig. 5 *B* ultimately closed, although its conductance had exceeded ~12 nS for ~1 s.

Comparison of experimental results with theoretical predictions

The electrically detectable property of the fusion pore is its conductance that evolves in a characteristic manner. Fusion pore conductance increases from zero to an immeasurably large value in <15 ms for 8% of all observable fusion events (Monck et al., 1991). For all other fusion pores, the first indication of pore formation is an abrupt increase in fusion pore conductance from zero to a finite value. Fusion pore conductance then continues to either increase or to fluctuate about some value. The conductance of fluctuating fusion pores finally either returns to zero or increases to an immeasurably large value. Like the initial event, the final event is abrupt. Here we show that energetic considerations alone predict that lipidic pores can evolve in the same manner.

Initial stages

Electrically, the first indication of the formation of the exocytotic fusion pore is the abrupt increase in conductance to a finite value. The smallest initial conductance observed for exocytotic fusion pores is ~200 pS (Spruce et al., 1990). To calculate the corresponding minimum initial conductance of a lipidic pore, we assumed that ions crossed the pore without encountering any barriers or filters. A conducting lipidic pore would have to be large enough to allow a hydrated ion through. The initial conductance would then coincide with the radius of this lipidic pore meeting or exceeding this required minimum radius (0.2–0.3 nm). Assuming the radius of a sin-

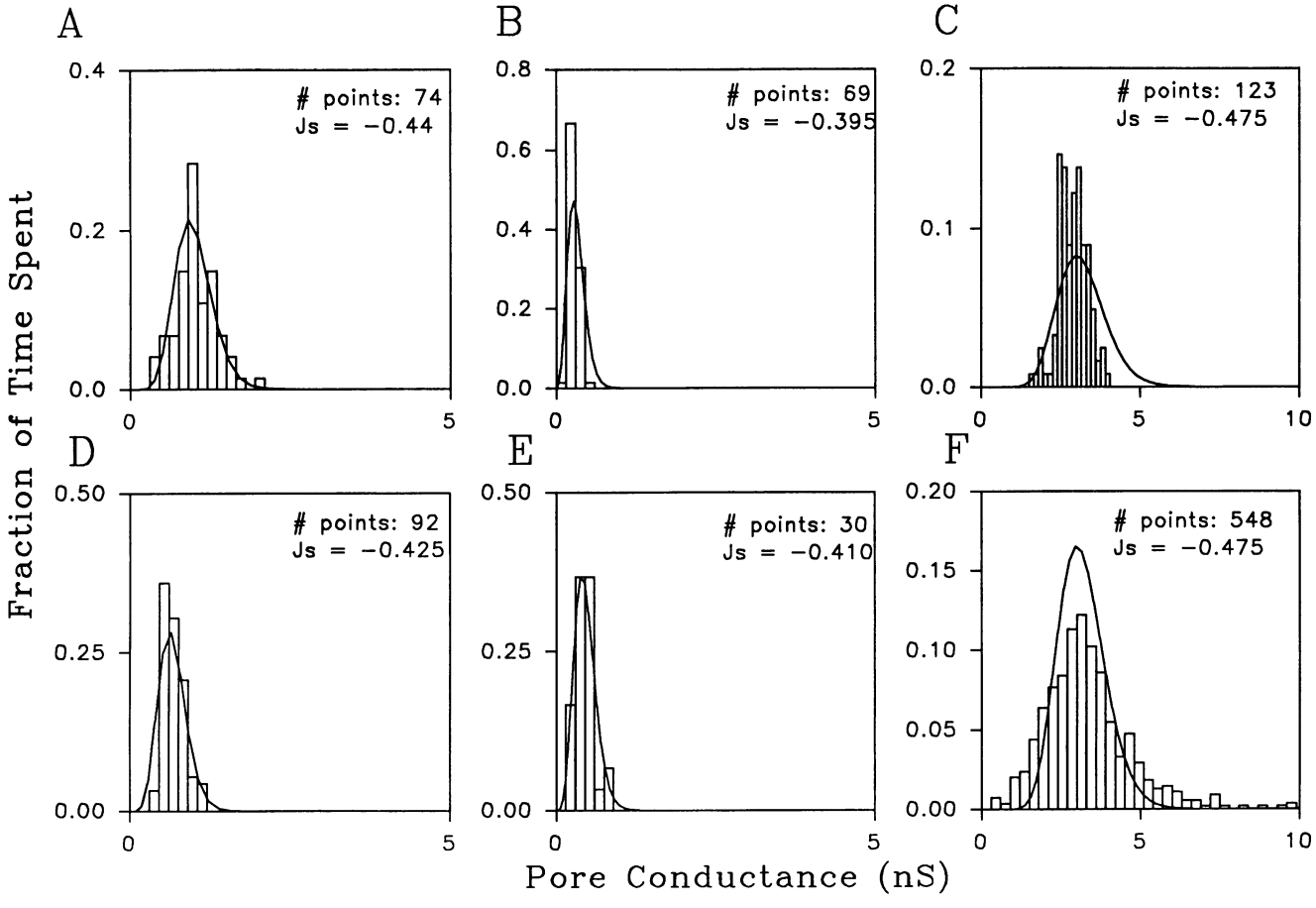

FIGURE 7 Comparison of theoretical predictions with experimental data for transient fusion events. Fusion pore conductance histograms (*bars*) for six transient events were fit to theoretically predicted distributions (*continuous curves*) assuming a pore in a bilayer. Format is the same as Fig. 6 except that the bin width was 150 pS for all events except the one shown in Fig. 7 *F* (300 pS bins). The distributions shown in Figs. 6 *B* and 7 *C* are from an irreversible and a transient fusion event in the same cell, whereas the distributions of 7 *A* and *B* are from two different transient fusion events from one cell. All the other distributions are from different cells.

gle lipid headgroup is 0.4 nm, the radius of a pore lined by five lipids is 0.25 nm with a pore conductance of 131 pS (Eq. 1).

Intermediate stages

Between the time that the fusion pore was first detectable electrically and the time that it ceased to do so, the conductance of the fusion pore either increased monotonically or fluctuated about some value. Lipidic pores will continue to expand when it is energetically favorable to do, i.e., when an increase in pore radius results in a decrease in free energy. Fig. 2 *C* shows that when the lipid composition is such that the spontaneous curvature of the lipids lining the pores is <-0.5 nm^{-1}, pore free energy decreases monotonically, indicating expansion of a lipidic pore. The rate at which the conductance increases depends both on the tension and on the spontaneous curvature. Stable lipidic pores with a mean radius of r_p are energetically favorable if r_p corresponds to a local minimum in pore free energy. For lipidic pores with spontaneous curvatures between -0.3 and -0.5 nm^{-1}, the free energy displays the required minimum (Fig. 2 *B*, curve *2*). Random changes in thermal energy around the minimum result in a fluctuating radius and conductance.

As shown in Fig. 5, the size of the fluctuations in fusion pore conductance are correlated with and distributed around the mean conductance. We extended this analysis to compare the conductance distributions (about an equilibrium value) for a fusion pore with those of a lipidic pore. Figs. 6 and 7 show the conductance distributions for 12 fusion pores that met the criteria defined in Methods. These 12 examples were selected to show the variability in the mean, variance, and conductance distributions between cells and within a given cell. To compare theoretical conductance distributions with data, we used Eq. A.13 to calculate conductance distributions for a lipidic pore spanning a single 4-nm bilayer. Distributions with different means were calculated by varying the spontaneous curvature keeping all the other parameters fixed. By changing J_s between -0.395 and -0.475 nm^{-1}, we generated conductance

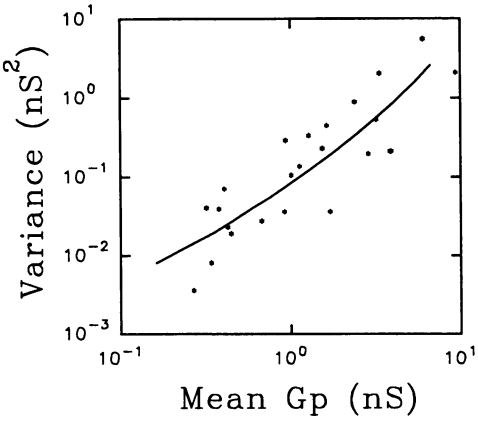

FIGURE 8 Variance versus mean for quasi-steady-state pores. Data from both transient and irreversible events have been included (*asterisks*). Solid curve is a theoretically predicted variance-mean relationship obtained by varying J_s ($\gamma = 0.1$ mN/m, $k_c = 1 \times 10^{-12}$ ergs, $h = 2$ nm; pore spans a single bilayer). The mean conductance of the largest stable pores was 6.7 nS.

distributions for lipidic pores with mean conductances between 400 pS and 5 nS. The predicted distributions for a lipidic pore are superimposed on the distributions for exocytotic fusion pores. We found that different values of J_s were necessary to fit the conductance distributions for different events within a single cell (Fig. 7, *A* and *B*, or Figs. 6 *B* and 7 *C*).

Fluctuation analysis of stable fusion pores

For fluctuating exocytotic fusion pores, the variance of the conductance fluctuations depends on the mean conductance (Figs. 5–7). What types of molecular events would give rise to such fluctuations? One possibility is that the fusion pore is a multistate channel. These fluctuations would then reflect transitions between different levels. If the fluctuations were simply due to fluctuations of an ion channel making transitions between two conductance levels (conductance g_1 and g_2; probability of occurrence, p_1 and $p_2 = [1 - p_1]$), the variance, σ_g^2 would be given by

$$\sigma_g^2 = p_1 p_2 (g_1 - g_2)^2. \quad (4)$$

The variance is zero when the channel is always in one or the other state ($p_1 = 0$ or $p_2 = 0$), and it peaks when the channel is in each state for 50% of the time. The variance will display a similar peak even for a more complicated multistate channel. Fig. 8 shows the variance as a function of mean conductance for 24 different fusion pores (*asterisks;* both transient and irreversible events are included). The variance in conductance increases as the mean conductance increases. For mean conductances up to 8 nS, the variance-mean relationship of the data does not display the peak that is predicted if the fluctuations arose from transitions between two closely spaced conducting levels of a single channel. Although it is possible that this peak occurs at a mean conductance ≥ 8 nS, this would imply a single-channel conductance ≥ 16 nS. Such large protein channels have not yet been described.

These fluctuations could also arise from thermal fluctuations in pore radius or from diffusional changes in lipid composition and spontaneous curvature. For a lipidic pore of the type considered here, we can calculate the variance-mean relationship from the predicted form of the conductance distributions, assuming thermal fluctuations in pore radius give rise to the conductance fluctuations. The solid curve in Fig. 8 shows the predicted variance-mean relationship for a lipidic pore through a single bilayer. The mean conductance was varied by varying J_s, keeping all other parameters fixed ($k_c = 1 \times 10^{-12}$ ergs; $\gamma = 0.1$ mN/m). The theoretical predictions agree with the experimental data. Increasing the tension shifts the predicted variance-mean relationship to the left (not shown). This is predicted by Fig. 2 *B*, which shows that tension increases the width of the energy well and therefore the variance, without significantly changing the equilibrium radius that determines the mean.

Final stages

In its final stages, the conductance of a fluctuating fusion pore abruptly increases or returns to zero. Fig. 2 *B*, curve *2*, displays an energy dependence consistent with an abrupt increase in pore conductance. The energy has a minimum and a maximum that correspond to a local equilibrium state and an energy barrier, respectively. Once the random thermal energy of a lipidic pore exceeds the barrier energy, the pore expands irreversibly since free energy now decreases as radius increases. Since the pore radius increases suddenly on overcoming this barrier, this would manifest itself as an abrupt increase in pore conductance.

DISCUSSION

Multisubunit ion channels intrinsically possess the properties of the early exocytotic fusion pore, since they can open abruptly, close, and fluctuate between different conductance levels. Almers (1990) therefore proposed that the early fusion pore was a proteinaceous ion channel. However, it has not been clear that it is at all necessary to invoke an ion channel-like structure to explain the properties of the early exocytotic fusion pore. In particular, does a lipidic pore such as the one that forms during bilayer fusion have the properties of the early exocytotic fusion pore? We showed in this paper that a lipidic pore, whose free energy was governed by an elastic component and tension, had all the electrical properties of the early fusion pore. Here we will discuss the validity of our model and the implications of our results.

Tension

We explicitly included the effects of tension in our model. Tension may be the driving force that results in

the transfer of lipid molecules from the cellular to the granular membrane (rate of $\sim 6 \times 10^5$ lipid molecules/s or a decrease in cell membrane area at a rate, dA/dt, of 0.16 $\mu m^2/s$) (Monck et al., 1990). To estimate the tension causing this flux, we equated the work done by tension in changing the granule area ($\gamma \delta A$) with the viscous energy dissipated ($\eta v \delta z$). Here v is the velocity of the lipids, η is the viscosity, δA is the change is granule area, and δz is the distance traversed by the lipid molecules. Tension, γ, is given by

$$\gamma = \frac{4\eta \frac{dA}{dt}}{\pi^4 r_p^2}. \quad (5)$$

Since viscosity ranges between 0.01 and 1 $\mu N \cdot s/m$ (Hochmuth et al., 1982; Waugh, 1982), the tension necessary to generate the observed flux of lipids through a 2-nm pore ranges between 0.003 and 0.3 mN/m. Changes in tension affect the widths of the conductance distributions without significantly altering any of the conclusions drawn here. Instead of complicating the analysis by varying the tension and introducing an additional free parameter, we chose a constant tension (0.1 mN/m) and changed spontaneous curvature, the major determinant of mean conductance, to perform the fits.

Previous models for lipidic pores, which included the effects of curvature energy alone, predicted that lipidic pores could fail to form, open and continue expanding, or open with a radius equal to some equilibrium radius (Markin et al., 1984). Changes of spontaneous curvature were necessary to explain the final irreversible expansion of fluctuating lipidic pores influenced by curvature energy alone. By including tension, we found that fluctuating lipidic pores could expand irreversibly without requiring any changes in spontaneous curvature.

Choice of parameters affecting curvature energy

The curvature energy depends on pore geometry, spontaneous curvature, and bending modulus. Since the early fusion pore has not been directly visualized, there is no information on fusion pore geometry. In our analysis, we therefore chose a simple shape for the fusion pore. Lipid spontaneous curvature and bilayer bending modulus have been measured or estimated by various laboratories for different lipids (or mixtures). These data are summarized in Table 1. The values of J_s used to fit our data were between -0.395 and -0.475 nm^{-1} (or r_s = 2.1–2.5 nm) and are within the range of J_s reported for cellular lipids (Luzzati and Husson, 1962) or artificial phospholipids and mixtures (references in Table 1). Although the lipids lining the fusion pore are unknown, membrane destabilizing lipids are likely to be involved. We therefore chose a bilayer bending modulus of 4×10^{-12} ergs that was reported by Duwe et al. (1990) for a dimyristoyl-phosphatidylcholine-cholesterol mixture. For our calculations, we modeled the fusion pore as a lipidic pore through a single bilayer. The appropriate modulus is therefore the monolayer modulus that is one fourth of the modulus for a bilayer (Evans and Hochmuth, 1978). It is important to notice that tension and the bending modulus together determine the size of the largest stable pores. For instance, with a tension of 0.1 mN/m, monolayer bending moduli of 1 or 0.25×10^{-12} ergs result in stable pores with mean conductances that are <6.7 and <3.94 nS, respectively.

Stable or irreversibly expanding pores require spontaneous curvatures between -0.395 and -0.475 nm^{-1}. In artificial bilayer systems, these high spontaneous curvatures result in inverted cylinders. It is important, however, to keep in mind that these high spontaneous curvatures are necessary, not on the entire membrane, but only in small localized fusogenic spots or domains. These domains of membrane destabilizing lipids could support both irreversibly expanding pores and stably fluctuating pores without destabilizing the entire cell membrane. Increased levels of membrane destabilizing lipids, such as arachidonic acid and diacylglycerol, are observed after the stimulation of exocytosis (reviewed in Burger and Verkleij, 1990). Although arachidonic acid- or diacylglycerol-rich domains have not yet been reported, evidence supporting localized lipid domains have been reported for biological membranes (Yechiel and Edidin, 1987; Tocanne et al., 1989; Rodgers and Glaser, 1991).

Implications of lipid domains

The fusion pore conductance distributions shown in Fig. 7, *A* and *B*, are from transient fusion events in the same cell. As shown by the mean and spread of the distributions, the underlying fusion pores display very different behavior. Within the framework of the model presented here, these changes could be attributed to changes in the composition of the lipids making up the pores. Minor changes in the lipid composition of cell extracts have been shown to result in changes in spontaneous curvature (Luzzati and Husson, 1962).

The conductance of some fusion pores fluctuated around two or more different quasi-stable states before the pore either closed or expanded irreversibly. For such pores, the pore conductance initially fluctuates around one value and then abruptly starts fluctuating about a new value (e.g., Fig. 4 *B*). A lipidic pore of the type described here has, for a constant spontaneous curvature, at most one energy minimum that corresponds to a single stable conductance state. Multiple stable states might, however, be a consequence of a flux-induced change in lipid composition and therefore J_s. Such changes would result in a pore whose conductance apparently exhibits several states. Multiple conductance states could also be explained by the formation of several fusion pores that could connect the membrane of a single granule to the plasma membrane. Chandler and

TABLE 1 **Values of parameters used in the model**

Parameter	Variable	Value used here	Range
Bilayer bending modulus	k_c	4×10^{-12} ergs	$0.7–4 \times 10^{-12}$ ergs*
Spontaneous curvature	J_s	-0.475 to -0.395 nm^{-1}	-2 to -0.2 nm^{-1} ‡
Viscosity	η		0.01–1 μN · s/m§
Tension	γ	0.1 mN/m‖	0.003–0.3 mN/m‖

* Schneider et al., 1984; Bo and Waugh, 1989; Duwe et al., 1990; Mutz and Helfrich, 1990. ‡Luzzati and Husson, 1962; Tate and Gruner, 1987; Rand et al., 1990; Leventis et al., 1991. §Waugh, 1982; Hochmuth et al., 1982. ‖As discussed in the text, γ depends on r_p and η. The range given here is for a 2-nm pore.

Heuser's (1980) freeze-fracture photographs suggest that two to four pores could be formed between the granular and plasma membranes in degranulating mast cells.

Closure of a lipidic pore

Electrophysiological data from degranulating mast cells showed that fusion pores could close within milliseconds to seconds of opening (Fernandez et al., 1984). This was unexpected since it implied that perhaps fusion was reversible. Can a lipidic pore of the type considered here also close? Electrically induced pores through bilayers and cells close within microseconds to minutes of removal of the electric field (Benz and Zimmermann, 1981; Chang and Reese, 1990). For the lipidic pores described in this paper, spontaneous curvature determines the type of pores formed. We assumed that spontaneous curvature was constant during the lifetime of the pore. On the basis of energetic considerations alone, for a fixed spontaneous curvature, a stable fluctuating pore will not close since the equilibrium radius corresponds to the local minimum for energy (Fig. 2 *B*). However, the tension-mediated flow of lipids through a conducting pore could result in the replacement of pore-forming lipids by non–pore-forming lipids. This will change the spontaneous curvature, allowing a fusion pore to close while leaving a pore-free hemifusion bilayer. A similar mechanism could be used to explain the irreversible expansion of a fluctuating pore. Oberhauser et al. (1992) had used a similar argument when they suggested that the sharp decrease in the rate of fusion pore closure in mast cells cooled to below 13°C was due to the phase-separation and subsequent removal of a closure favoring lipid.

The putative role of proteins in the formation of a lipidic exocytotic fusion pore

In this paper, we have demonstrated that a lipidic pore shares the properties of the electrically measurable exocytotic fusion pore. It then remains to understand how such a lipidic pore could form between the well-separated plasma and secretory granule membrane. In mast cells, the formation of a fusion pore and the resulting secretion of granule contents can be triggered by the application of intracellular GTPγS alone (Fernandez et al., 1984). This suggests that proteins are involved in regulating the formation of the fusion pore. Various models have been put forward to depict the role of proteins in the formation of a lipidic pore. Ornberg and Reese (1981) suggest that contractile proteins pull the plasma and granule membranes together, resulting in the formation of a lipidic pore spanning two bilayers. White (1990), on the other hand, suggests that proteins that connect the membranes being fused form a hydrophobic surface that allows lipids to flow from one membrane to the other, resulting in complete fusion. Based on our data and the results of bilayer fusion experiments, we suggest that at rest, a scaffold of proteins connects the granule and the plasma membranes (Nanavati et al., 1992). On activation, this scaffold draws the granule and plasma membranes together at a narrow focal point, bypassing the short-range repulsive interbilayer hydration forces. The two closely apposed, highly curved membranes fuse into a single bilayer in much the same way as two tensed or depleted phospholipid bilayers fuse to form a hemifused bilayer (Helm et al., 1992). A pore formed in this bilayer can, as shown in this paper, expand irreversibly, fluctuate, or close. Pore opening itself is a reversible event, although hemifusion, or formation of the hemifused bilayer, is not.

This model provides a simple mechanism that explains the existence of transient fusion pores that can open several times. For instance, Spruce et al. (1990) analyzed the conductance of a fusion event in which a fusion pore opened and closed eight times before expanding irreversibly. They found that the kinetics and the conductance differed from opening to opening. According to the simple model presented here, on closure of a fusion pore, a new pore would form in the hemifused bilayer if membrane tension and lipid composition favor pore formation. The spontaneous curvature and therefore the behavior of each new pore is likely to be different since the lipid composition is not constant within a cell. Yet, each of these pores connects the lumen of the same granule to the extracellular space. In this model, the steps that require the overcoming of interbilayer forces and the formation of a hemifused bilayer are irreversible, whereas pore opening is reversible.

In this paper, we have shown that a lipidic pore, whose behavior is governed by spontaneous curvature and membrane tension, has the properties of the early exocytotic fusion pore. This model predicts that interventions

that affect these two parameters must affect the behavior of the fusion pore. Spontaneous curvature can be changed by changing lipid composition or by introducing amphipaths (Chernomordik et al., 1992). Membrane tension can be changed by introducing amphipaths that selectively partition into one or the other monolayer (Martinac et al., 1990) or by applying a transmembrane electric field that will introduce an effective electrocompressive force on the membrane (Needham and Hochmuth, 1989). All these predictions can be tested using the methods outlined in this paper.

APPENDIX

For our calculations, we assumed the pore was generated by revolving a half-circle of radius b around an external axis at a distance a, thus generating a section of a toroid (Fig. 1 *A*). The shortest distance between any point on the circle and the axis of revolution was x. The surface generated by revolving the curve of Fig. 1 *A* corresponds to the neutral surface (*dashed lines* in Fig. 1, *B* and *C*). The variables a and b are related to pore parameters radius (r), bilayer thickness ($2h$), and interbilayer distance (d) by

$$a = r + h/2; \quad b = h/2$$

for a pore spanning one bilayer; (A.1a)

$$a = r + h; \quad b = h + d/2$$

for a pore spanning two bilayers. (A.1b)

In the derivations that follow, we make no distinction between a pore spanning a single bilayer or two bilayers. However, all the numerical examples considered here are for a pore spanning a single, 4-nm-thick bilayer.

Pore conductance

The resistance, dR, of an infinitesimal cylindrical pore of resistivity ρ, area $A = \pi x^2$, and length, dy, is given by:

$$dR = \rho \frac{dy}{\pi x^2}. \tag{A.2}$$

For a pore with the geometry of Fig. 1, *B* or *C*, x is given by

$$x(y) = r + \frac{L}{2} - \sqrt{\frac{L^2}{4} - y^2},$$

where $L = 4h + d$ or $2h$. Substituting and integrating Eq. A. 2, we get

$$R_{\text{pore}} = \frac{\rho}{\pi} \frac{L}{r(r+L)} \times \left\{1 + \frac{L}{\sqrt{r(r+L)}} \arctan \sqrt{\frac{r+L}{r}}\right\}. \tag{A.3a}$$

The total resistance of the pore must include the access resistance that we approximated as (Hille, 1992)

$$R_{\text{access}} = \frac{\rho}{2r + L}. \tag{A.3b}$$

Pore conductance, G_p, the inverse of the total resistance is

$$G_p = \frac{1}{R_{\text{pore}} + R_{\text{access}}}. \tag{A.3c}$$

Curvature elastic energy of a pore

Following Markin et al. (1984), we calculated the energy by integrating the curvature energy per unit area over the surface of revolution. The change in bending energy on pore formation is the difference between the elastic energy in the absence and presence of a pore. The elastic bending energy per unit area of a bilayer without a pore is

$$\frac{1}{2} k_c J_s^2, \tag{A.4a}$$

and the energy in the presence of a pore is

$$\frac{1}{2} k_c (J_m + J_p - J_s)^2, \tag{A.4b}$$

where k_c is the bending rigidity or elasticity modulus, J_s is the spontaneous curvature, and J_m and J_p are the meridional and parallel curvatures, respectively. If $\psi(x)$ is the angle between the tangent line and the horizontal (*inset*, Fig. 1 *A*), then

$$\tan \psi = \frac{dy}{dx},$$

where $y(x)$ is the equation of the generating semicircle (*inset*, Fig. 1 *A*). The curvatures are then given by

$$J_m = \cos \psi \frac{d\psi}{dx}$$

$$J_p = \frac{\sin \psi}{x}.$$

For this particular geometry,

$$J_m = -\frac{1}{b}. \tag{A.5a}$$

Furthermore, since

$$x + b \sin \psi = a + b,$$

we get

$$\sin \psi = \frac{a + b - x}{b};$$

therefore,

$$J_p = -\frac{1}{b}\left(1 - \frac{b+a}{x}\right). \tag{A.5b}$$

The curvature energy is then given by

$$W_b = \frac{1}{2} k_c \int \left[\left(-\frac{2}{b} + \frac{b+a}{x} - J_s\right)^2 - J_s^2\right] dA, \tag{A.5c}$$

where the area of an infinitesimal surface, dA, is

$$dA = 2\pi x \sqrt{1 + (x')^2}\, dy, \tag{A.6}$$

$$x = (a + b) - \sqrt{b^2 - y^2},$$

and $x'(y) = dx/dy$. Integrating Eq. 5c, we get the bending energy, W_b, as

$$W_b = 2\pi k_c \left\{\pi J_s a + \frac{2(b+a)^2}{b\sqrt{a(a+2b)}} \arctan \sqrt{\frac{a+2b}{a}} + \left(\frac{\pi}{2} - 4\right) b J_s - 4\right\}. \tag{A.7}$$

This expression for energy is itself not very enlightening. To gain some insight into the dependence of energy on radius, we considered the extreme cases of large or small radii. For a pore spanning a single bilayer, these are equivalent to ($a \gg b$) and to ($r \to 0$, $a \to h/2$), respectively. When $a \gg b$, Eq. A.7 simplifies to

$$W_b = 2\pi k_c \pi \left(J_s + \frac{1}{2b} \right) a,$$

i.e., the bending energy is a linear function of radius. For $J_s > -1/2b$, energy increases with increasing radius, whereas for $J_s < -1/2b$, energy decreases with increasing radius.

For small radii, the bending energy is also a linear function of pore radius with a slope, dW_b/da, given by

$$\frac{dW_b}{da} = 2\pi k_c \left\{ \pi J_s + \frac{2}{b} \frac{(a^3 + 3a^2b + ab^2 - b^3)}{(a^2 + 2ab)^{3/2}} \times \arctan \sqrt{\frac{a+2b}{a}} - \frac{2(a+b)}{(a^2+2ab)} \right\}.$$

For $a \to h/2$, this slope is positive for those spontaneous curvatures that satisfy

$$\pi J_s > \frac{2}{b} \frac{(a^3 + 3a^2b + ab^2 - b^3)}{(a^2 + 2ab)^{3/2}} \times \arctan \sqrt{\frac{a+2b}{a}} - \frac{2(a+b)}{(a^2+2ab)}.$$

For a small pore through a 4-nm-thick bilayer, $b = h/2$, $a = h/2$ implies that for $J_s > -0.3$ nm^{-1}, the energy of small pores increases as the radius increases, whereas for $J_s < -0.3$ nm^{-1}, energy decreases as the radius increases. To summarize, for large radii, the slope, dW_b/da, is positive for $J_s > -0.5$ nm^{-1} and negative for $J_s < -0.5$ nm^{-1}. For small radii, the slope is positive for $J_s > -0.3$ nm^{-1} and negative for $J_s < -0.3$ nm^{-1}. Therefore, for spontaneous curvatures between -0.3 and -0.5 nm^{-1}, the slope is negative for small radii and positive for large radii. This implies that W_b has a minimum at some intermediate radius when J_s lies between -0.5 and -0.3 nm^{-1}.

Work done by tension

$W_{tension}$, the contribution of tension, γ, to the free energy is

$$W_{tension} = \gamma \delta A, \qquad (A.8)$$

where δA is the change in membrane area as a result of tension. The application of tension results in the formation of a "hole" of radius, "$a + b$," and area, A_h (Fig. 1 *A*),

$$A_h = 2\pi(a+b)^2,$$

(where the factor of 2 accounts for the two sides of the bilayer) and the formation of a pore with membrane area, A_p. A_p is the area of the surface of revolution generated by revolving the semicircles of Fig. 1 *A* and is calculated by integrating Eq. A.6, which yields

$$A_p = 2\pi[\pi b(a+b) - 2b^2]. \qquad (A.9)$$

δA is the difference between A_p and A_h. So, $W_{tension}$ is given by

$$W_{tension} = -2\pi\gamma(a^2 - (\pi - 3)b^2 - (\pi - 2)ab). \qquad (A.10)$$

The free energy is the sum of W_b and $W_{tension}$.

Distribution of pore conductances

Assuming pore radii are distributed according to a Boltzmann distribution, the probability of observing a pore of radius between r and $r + dr$ is

$$p(r)dr = \frac{1}{B} \exp\left[-\frac{w(r)}{k_B T} \right] dr \qquad (A.11)$$

$$B = \int_0^\infty \exp\left[-\frac{w(r)}{k_B T} \right] dr, \qquad (A.12)$$

where k_B = Boltzmann's constant and T = absolute temperature.

To compare the experimentally obtained distributions of pore conductance, we transformed the distribution of pore radii to a distribution of pore conductances using

$$p(G_p)dG_p = p(r(G_p)) \left(\frac{dG_p}{dr} \right)^{-1} dG_p, \qquad (A.13)$$

where $p(G_p)dG_p$ = the probability of observing a pore of conductance between G_p and $G_p + dG_p$ and $r(G_p)$ is given by inverting Eq. A.3c.

We are grateful to Drs. W. Helfrich (Freie Universitat, Berlin), A. Herrmann (Humboldt Universitat), J. Kas (Technische Universitaat, Munchen), J. R. Monck (Mayo Foundation), D. Needham (and the members of his laboratory; Duke University), and S. Simon (Duke University) for useful comments. This work was supported by National Institute of Health grants to J. M. Fernandez, who is also an Established Investigator for the American Heart Association.

Received for publication 23 January 1992 and in final form 7 May 1992.

REFERENCES

Almers, W. 1990. Exocytosis. *Annu. Rev. Physiol.* 52:607–624.

Alvarez de Toledo, G., and J. M. Fernandez. 1988. The events leading to secretory granule fusion. *In* Cell Physiology of Blood. R. B. Gunn and J. C. Parker, editors. Society of Gen Physiol Series. Vol. 43. The Rockefeller University Press, New York. 333–344.

Alvarez de Toledo, G., and J. M. Fernandez. 1990. Patch-clamp measurements reveal multimodal distribution of granule sizes in rat mast cells. *J. Cell Biol.* 110:1033–1039.

Benz, R., and U. Zimmerman. 1981. The resealing process of lipid bilayers after reversible electrical breakdown. *Biochim. Biophys. Acta.* 640:169–178.

Bo, L., and R. E. Waugh. 1989. Determination of bilayer membrane bending stiffness by tether formation from giant, thin-walled vesicles. *Biophys. J.* 55:509–517.

Breckenridge, L. J., and W. Almers. 1987. Currents through the fusion pore that forms during exocytosis. *Nature (Lond.).* 328:814–817.

Burger, K. N. J., and A. J. Verkleij. 1990. Membrane fusion. *Experientia.* 46:631–644.

Chandler, D. E., and J. E. Heuser. 1980. Arrest of membrane fusion events in mast cells by quick-freezing. *J. Cell Biol.* 86:666–674.

Chang, D. C., and T. S. Reese. 1990. Changes in membrane structure induced by electroporation as revealed by rapid-freezing electron microscopy. *Biophys. J.* 58:1–12.

Chernomordik, L. V., S. S. Vogel, E. Leikina, and J. Zimmerberg. 1992. Inhibition of biological membrane fusion by amphipathic compounds. *Biophys. J.* 61:499*a*. (Abstr.)

Deuling, H. J., and W. Helfrich. 1976. The curvature elasticity of fluid membranes: a catalogue of vesicle shapes. *J. Physique.* 37:1335–1345.

Deuling, H. J., and W. Helfrich. 1977. A theoretical explanation for the myelin shapes of red blood cells. *Blood Cells.* 3:713–720.

Duwe, H. P., J. Kaes, and E. Sackmann. 1990. Bending elastic moduli of lipid bilayers: Modulation by solutes. *J. Physique.* 51:945–962.

Evans, E. A., and R. M. Hochmuth. 1978. Mechanochemical properties of membranes. *In* Current Topics in Membranes and Transport. F. Bronner, and A. Kleinzeller, editors. Academic Press, New York. 1–64.

Fernandez, J. M., E. Neher, and B. D. Gomperts. 1984. Capacitance measurements reveal stepwise fusion events in degranulating mast cells. *Nature (Lond.).* 312:453–455.

Fidler, N., and J. M. Fernandez. 1989. Phase tracking: an improved phase detection technique for cell membrane capacitance measurements. *Biophys. J.* 56:1153–1162.

Hamill, O. P., A. Marty, E. Neher, B. Sakmann, and F. J. Sigworth. 1981. Improved patch-clamp techniques for high-resolution current recording from cells and cell-free membrane patches. *Pfluegers Arch. Eur. J. Physiol.* 391:85–100.

Helfrich, W. 1973. Elastic properties of lipid bilayers: theory and possible experiments. *Z. Naturforsch.* 28:693–703.

Helm, C. A., J. N. Israelachvili, and P. M. McGuiggan. 1992. Role of hydrophobic forces in bilayer adhesion and fusion. *Biochemistry.* 31:1794–1805.

Hille, B. 1992. Ionic Channels in Excitable Membranes. Sinauer Associates, Inc., Sunderland, MA. 296.

Hochmuth, R. M., H. C. Wiles, E. A. Evans, and J. T. McCown. 1982. Extensional flow of erythrocyte membrane from cell body to elastic tether. II. Experiment. *Biophys. J.* 39:71–81.

Joshi, C., and J. M. Fernandez. 1988. Capacitance measurements: an analysis of the phase detector technique used to study exocytosis and endocytosis. *Biophys. J.* 53:885–892.

Kas, J., and E. Sackmann. 1991. Shape transitions and shape stability of giant phospholipid vesicles in pure water induced by area-to-volume changes. *Biophys. J.* 60:825–844.

Leventis, R., N. Fuller, R. P. Rand, P. L. Eagle, A. Sen, M. J. Zuckermann, and J. R. Silvius. 1991. Molecular organization and stability of hydrated dispersion of headgroup-modified phosphatidylethanolamine analogues. *Biochemistry.* 30:7212–7219.

Luzzati, V., and F. Husson. 1962. The structure of the liquid-crystalline phases of lipid-water systems. *J. Cell Biol.* 12:207–219.

Markin, V. S. 1981. Lateral organization of membranes and cells shapes. *Biophys. J.* 36:1–19.

Markin, V. S., M. M. Kozlov, and V. L. Borovjagin. 1984. On the theory of membrane fusion. The stalk mechanism. *Gen. Physiol. Biophys.* 3:361–377.

Martinac, B., J. Adler, and C. Kung. 1990. Mechanosensitive ion channels of *E. coli* activated by amphipaths. *Nature (Lond.).* 348:261–263.

Monck, J. R., G. Alvarez de Toledo, and J. M. Fernandez. 1990. Tension in secretory granule membranes causes extensive membrane transfer through the exocytotic fusion pore. *Proc. Natl. Acad. Sci. USA.* 87:7804–7808.

Monck, J. R., A. F. Oberhauser, G. Alvarez de Toledo, and J. M. Fernandez. 1991. Is swelling of the secretory granule matrix the force that dilates the exocytotic fusion pore? *Biophys. J.* 59:39–47.

Mutz, M., and W. Helfrich. 1990. Bending rigidities of some biological model membranes as obtained from the Fourier analysis of contour sections. *J. Physique.* 51:991–1002.

Nanavati, C., V. S. Markin, A. F. Oberhauser, and J. M. Fernandez. 1992. The exocytotic fusion pore as a protein-supported lipidic structure. *Biophys. J.* 61:421*a*. (Abstr.)

Needham, D., and R. M. Hochmuth. 1989. Electro-mechanical permeabilization of lipid vesicles role of membrane tension and compressibility. *Biophys. J.* 55:1001–1009.

Oberhauser, A. F., J. R. Monck, and J. M. Fernandez. 1992. The events leading to the opening and closing of the exocytotic fusion pore have markedly different temperature dependencies. A kinetic analysis of single fusion events in patch-clamped mouse mast cells. *Biophys. J.* 61:800–809.

Ornberg, R. L., and T. S. Reese. 1981. Beginning of exocytosis captured by rapid-freezing of *Limulus* amebocytes. *J. Cell Biol.* 90:40–54.

Rand, R. P., N. L. Fuller, S. M. Gruner, and V. A. Parsegian. 1990. Membrane curvature, lipid segregation, and structural transitions for phospholipids under dual-solvent stress. *Biochemistry.* 29:76–87.

Rodgers, W., and M. Glaser. 1991. Characterization of lipid domains in erythrocyte membranes. *Proc. Natl. Acad. Sci. USA.* 88:1364–1368.

Schneider, M. B., J. T. Jenkins, and W. W. Webb. 1984. Thermal fluctuations of large cylindrical phospholipid vesicles. *Biophys. J.* 45:891–899.

Siegel, D. P. 1986. Inverted micellar intermediates and the transitions between lamellar, cubic, and inverted hexagonal lipid phases. II. Implications for membrane-membrane interactions and membrane fusion. *Biophys. J.* 49:1171–1183.

Song, L., Q. F. Ahkong, D. Georgescauld, and J. A. Lucy. 1991. Membrane fusion without cytoplasmic fusion (hemi-fusion) in erythrocytes that are subjected to electrical breakdown. *Biochim. Biophys. Acta.* 1065:54–62.

Spruce, A. E., L. J. Breckenridge, A. K. Lee, and W. Almers. 1990. Properties of the fusion pore that forms during exocytosis of a mast cell secretory vesicle. *Neuron.* 4:643–654.

Tate, M. W., and S. M. Gruner. 1987. Lipid polymorphism of mixtures of dioleoylphosphatidylenthanolamine and saturated and monounsaturated phosphatidylcholines of various chain lengths. *Biochemistry.* 26:231–236.

Tocanne, J., L. Dupou-Cezanne, A. Lopez, and J. Tournier. 1989. Lipid lateral diffusion and membrane organization. *FEBS (Fed. Eur. Biochem. Soc.) Lett.* 257:10–16.

Waugh, R. E. 1982. Surface viscosity measurements from large bilayer vesicle tether formation. II. Experiments. *Biophys. J.* 38:29–37.

White, J. M. 1990. Viral and cellular membrane fusion proteins. *Annu. Rev. Physiol.* 52:675–697.

Yechiel, E., and M. Edidin. 1987. Micrometer-scale domains in fibroblast plasma membranes. *J. Cell Biol.* 105:755–760.